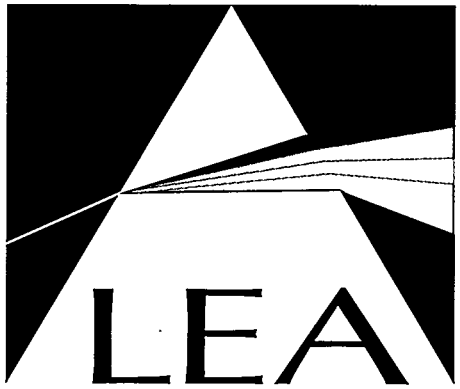

Laboratory for Experimental Astrophysics

UCRL-JC-119293

Non-equilibrium Dynamics in Superconducting Tunnel Junction Detectors

L.J. Hiller, Simon E. Labov, C.A. Mears, M. Frank, A.F. Bello
Laboratory for Experimental Astrophysics
Lawrence Livermore National Laboratory
P.O. Box 808, L-401, Livermore, CA 94550, USA

A.T. Barfknecht
Conductus, Inc.
969 West Maude, Ave., Sunnyvale, CA 94086, USA

Prepared for Proceedings, vol. 2280 of the
International Society of Optical Engineering 1994
July 24–29, 1994
San Diego, CA

December 9, 1994

DISCLAIMER

Portions of this document may be illegible in electronic image products. Images are produced from the best available original document.

Conf-940723--41

Non-equilibrium dynamics in superconducting tunnel junction detectors

L. J. Hiller, Simon E. Labov, C. A. Mears, M. Frank, A. F. Bello, A.T. Barfknecht*

Laboratory for Experimental Astrophysics,
Lawrence Livermore National Laboratory
P.O. Box 808, L-401, Livermore, CA 94550, USA

*Conductus, Inc., 969 West Maude Ave., Sunnyvale, CA 94086, USA

ABSTRACT

Superconducting tunnel junctions have the potential to serve as high-resolution, high-efficiency x-ray detectors for astrophysical and industrial applications. When irradiated by X rays, each X ray excites over 10^6 charge carriers which cause the detector to generate a pulse of current. We present an analysis of pulse shapes from detectors we have constructed and operated. We fit the decay of the current pulse to a simple model that considers two classes of carrier loss. One model considers only the normal recombination of the charge carriers with themselves, the other included additional losses due to recombination sites in the within the detector medium. We found that both mechanisms must be taken into account. We also found a small variation in pulse shape depending on which layer of the tunnel junction absorbed the X ray. We expect that this analysis will be a useful tool in comparing different detector designs and operating conditions.

1. INTRODUCTION

A superconducting tunnel junction (STJ) may be used as an energy dispersive X-ray detector by measuring the number of charge carriers, or quasiparticles, excited when an X ray is absorbed in one of the electrodes. Each X-ray photon breaks millions of pairs of superconducting electrons, or Cooper pairs, into excited states called quasiparticles. The quasiparticles diffuse through the absorber until recombining or tunneling across the barrier. The energy required to excite one pair of quasiparticles is the superconductor energy gap, commonly expressed as 2Δ, and is typically ~1 meV. When a bias voltage less than $2\Delta/e$ is applied to the junction these excited quasiparticles create a pulse of increased tunneling current through the oxide barrier. Since the energy to break a Cooper pair is of the order of 1 meV, ~10^6 quasiparticles are created for a 1 keV X ray. The large number of charge carriers reduces the effect of random fluctuations. The statistical limit for such a detector has been estimated to be ~4 eV at 6 keV,[1,2] with a resolving power ~30 times better than a semiconductor ionization detector. The best resolution achieved so far for an STJ detector is 36 eV (FWHM) at 6 keV.[3]

The performance of an STJ as an X-ray detector can be improved by using quasiparticle trapping.[4] A superconductor with a small energy gap, such as aluminum, is deposited on a superconductor with a large energy gap, such as niobium. When an X ray is absorbed in the niobium the excited quasiparticles diffuse through the absorber and into the aluminum. The quasiparticles quickly emit a phonon and relax to the gap edge of the aluminum layer, where they remain. Trapping the quasiparticles in the aluminum layer concentrates the quasiparticles near the tunneling barrier and thus enhances the tunneling rate. A second trapping layer on the opposite side of the barrier allows quasiparticles to also tunnel in the opposite direction. This form of reverse tunneling transfers charge in the forward direction while the net quasiparticle density shifts in the reverse direction.[5] Since quasiparticles can tunnel repeatedly until they recombine, the decay time of the current pulse corresponds to the quasiparticle lifetime.[6]

To recombine into a Cooper pair, each quasiparticle must recombine with another quasiparticle. Therefore, the self-recombination rate is proportional to the square of the quasiparticle density. Quasiparticles may also recombine or become trapped in regions of trapped magnetic flux, impurities, or normal metal. The rate of quasiparticles lost into these regions should be proportional to the quasiparticle density. In this paper we fit the decay of the pulse of tunneling current and relate its shape to the recombination rates of the quasiparticles.

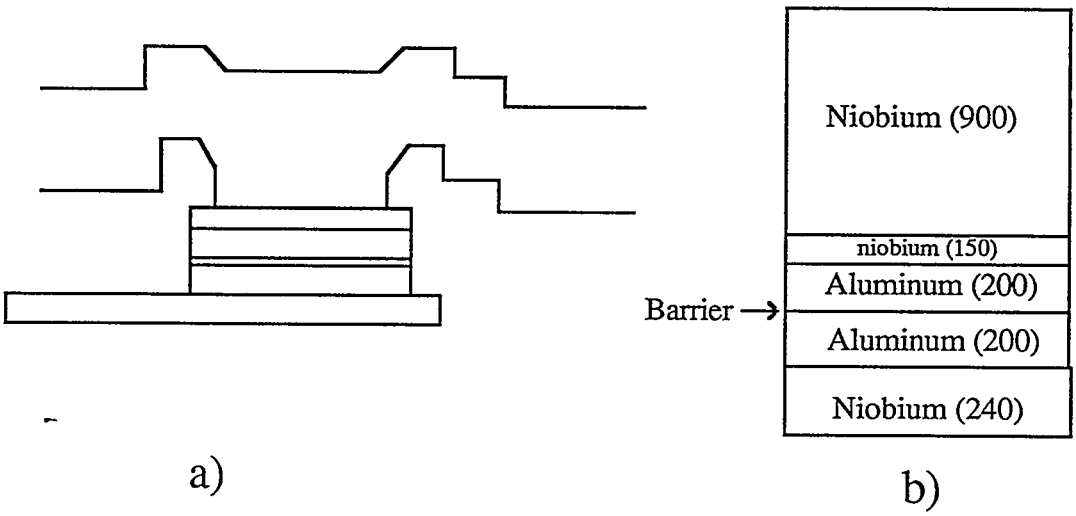

Fig. 1: a) The cross-section of the STJ detector discussed in this paper. b) A schematic diagram showing relative thicknesses of each layer in nm.

2. DETECTOR FABRICATION AND OPERATION

2.1 Detector fabrication

We fabricated several detectors at Conductus, Inc. using a modification of their photolithographic trilayer process.[7] A cross-section of one detector is shown in Fig. 1. We first covered a four-inch silicon wafer with SiO_2. A base electrode of niobium 240 nm thick was sputtered and then covered with a 200 nm aluminum layer. This was oxidized in a load lock to form the tunnel barrier. Another 200 nm aluminum layer and 150 nm niobium layer were then deposited. The detector was masked and the top niobium layer was removed by reactive ion etching. The aluminum layers were removed by wet etch. The base electrode was patterned with a photoresist and the unwanted niobium was removed. We then deposited an 800 nm layer of SiO_2 dielectric using plasma-enhanced chemical vapor deposition. The top niobium layer of the detector was cleaned with an ion mill and an additional 900 nm niobium absorbing layer was deposited. The detectors are diamond shaped and 100 μm on each side.

2.2. Detector operation

The detector analyzed in this paper was mounted in an adiabatic demagnetization refrigerator and cooled to below 100 mK. It is necessary to operate at this temperature to minimize the tunneling current due to thermally excited quasiparticles. The detector has been operated at up to 300 mK with only slightly degraded performance. A battery-powered magnetic field of 37.2 Gauss was applied in the plane of the detector to suppress the superconducting Josephson current through the barrier. The detector was then biased at 100 μV. The detector was irradiated by an ^{55}Fe source which emits Mn Kα and Kβ X rays at 5.89 and 6.49 keV respectively.

In order to study the current pulse shape directly, the current through the junction was measured using a negative feedback amplifier with a time constant of about 50 ns. Since the amplifier response is much less than the ~2 μs duration of the pulse, the amplifier output should be an accurate measurement of the current pulse. We chose to use a current-sensitive amplifier rather than the more traditional charge sensitive amplifier because the current-sensitive amplifier requires less dynamic range in the digitizing system to accurately measure the decay time of the current pulse. Unfortunately, our amplifying system

contains additional noise elements when operated in this mode. We are now in the process of improving these amplifiers.

3. DIGITAL PROCESSING

The output of the amplifier was digitized at 20 ns intervals. Pulse shape analysis was performed by fitting the current decay to the model described below. Pulse heights were determined by subtracting the average baseline current from the peak pulse height of the filtered pulse. This subtraction provides some rejection of low frequency 1/f noise.

3.1. Filtering

Filtering was performed by applying a Fast Fourier Transform (FFT) to the signal, multiplying by a response function, and taking the inverse FFT. This method has the advantage of speed and flexibility, since the response function can be an arbitrary function, compensate for amplifier distortion, or be an optimal noise filter. For our analysis, a gaussian-shaped non-causal low-pass filter function was used. This filter approximated the optimal filter and preserved the pulse shape while eliminating most of the high-frequency noise. While only the unfiltered pulse shape was fit, the filtered pulse shape was used to convey the quality of the fit.

3.2. Modeling

Our model includes two possible loss mechanisms. The first is self-recombination. For a nearly thermal distribution of quasiparticles with density n, the excess population relaxes at a rate given by :

$$\frac{dn}{dt} = -2\tau_r^{-1} n, \tag{1}$$

where τ_r^{-1} is the recombination rate for a single quasiparticle. The factor of 2 accounts for the loss of two quasiparticles in each recombination event. An expression for this rate is given by Kaplan *et al.*[8] in the low temperature limit:

$$\tau_r^{-1} = \frac{4\pi\Delta b(2\Delta)^2}{\hbar Z_1}\left(\frac{\pi kT}{2\Delta}\right)^{1/2} e^{\left(-\Delta/kT\right)}, \tag{2}$$

where b and Z_1 are material constants and τ_r^{-1} is the inverse recombination time. The temperature dependence in this expression can be replaced by the thermal quasiparticle density

$$n_{th} = 4N(0)\Delta\left(\frac{\pi kT}{2\Delta}\right)^{1/2} e^{\left(-\Delta/kT\right)}, \tag{3}$$

where N(0) is the single-spin density of states at the Fermi energy. We operated the device at extremely low temperature ($kT = 0.02\Delta$) so there is essentially no thermal quasiparticle density. However we believe that the athermal quasiparticles from an X-ray absorption relax to the gap edge. This narrow distribution sufficiently resembles the low-temperature thermal distribution that we may replace the thermal quasiparticle density n_{th} with the athermal quasiparticle density n used in the calculations of Kaplan *et al.*. Combining equations (1) through (3) we obtain an approximate expression for the recombination rate of a non-thermal population with energies near the gap edge:

$$\frac{dn}{dt} = -2\frac{4\pi b\Delta^2}{\hbar Z_1 N(0)} n^2 = -2\Lambda\Delta^2 n^2 \tag{4}$$

The value of Λ is a constant for each material. We refer to the quantity $\Lambda\Delta^2$ as the self-recombination coefficient. Using values from Kaplan *et al.*[8] and Chi and Clarke[9] we calculated $\Lambda = 1.39\times10^{-9}$ $cm^3s^{-1}meV^{-2}$. The presence of the niobium increases the gap in the aluminum and has a measured value of 0.72 meV. The theoretical value of the self-recombination coefficient $\Lambda\Delta^2$ is then 1.80×10^{-10} $cm^3s^{-1}meV^{-2}$. For simplicity, we have completely neglected to role of phonons in this process.

We expect an additional loss mechanism due to trapping in regions that were normal or had a suppressed energy gap. Each quasiparticle diffusing into such a region may emit a phonon and become trapped until it recombines. The loss rate for this process would then be proportional to the quasiparticle density. To account for this additional loss we included an additional term in (4):

$$\frac{dn}{dt} = -\tau_{loss}^{-1} n - 2\Lambda\Delta^2 n^2 \tag{5}$$

This differential equation has a solution

$$n(t) = \left(\frac{\tau_{loss}^{-1}}{2\Lambda\Delta^2}\right) \frac{e^{\left[-\tau_{loss}^{-1}(t-t_0)\right]}}{1 - e^{\left[-\tau_{loss}^{-1}(t-t_0)\right]}} \tag{6}$$

where t_0 is a time offset parameter. Since we do not have an estimate for the loss rate due to unwanted trapping, we consider the limit where self-recombination is dominant. The athermal quasiparticle density as a function of time is then

$$n(t) = \left[2\Lambda\Delta^2(t - t_0)\right]^{-1} \tag{7}$$

where t_0 is again a time offset.

We assume the current measured through the barrier, I_{tun}, was directly proportional to the quasiparticle density in the aluminum trapping layers:

$$n = 2eN(0)R_n I_{tun}. \tag{8}$$

where R_n is the normal resistance of the junction, about 0.1 Ω, and N(0) is the density of states for aluminum. We do not include the dependence on the bias voltage commonly included here, because the proximity effect eliminates the singularity in the BCS density of states at the band edge. This factor is expected to be of order unity.

4. RESULTS AND DISCUSSION

We analyzed our digitized signals by fitting the decay of each current pulse to a model using a non-linear fitting routine (Marquardt). The decay curve was fit to the models in equations (6) and (7). From both models a value for $\Lambda\Delta^2$ was computed and compared to the theoretical value calculated from material constants.

4.1 Self-recombination only model

First we considered the case where self-recombination was the only loss mechanism. Figure 2 shows the best fit of equation (7) to a sample pulse which has been smoothed to better illustrate the pulse shape. The simple model is unable to follow the decay exactly. To look for variations in the pulse shape with amplitude we plotted $\Lambda\Delta^2$ computed from the fit against pulse height. This is shown in Fig. 3. The points of very low amplitude are the result of the digitizing equipment triggering on noise rather than actual pulses. The recombination coefficient $\Lambda\Delta^2$ is not constant, which is counter to the expected result. Its value varies inversely with the pulse height. This can be seen clearly by plotting the product of $\Lambda\Delta^2$ with

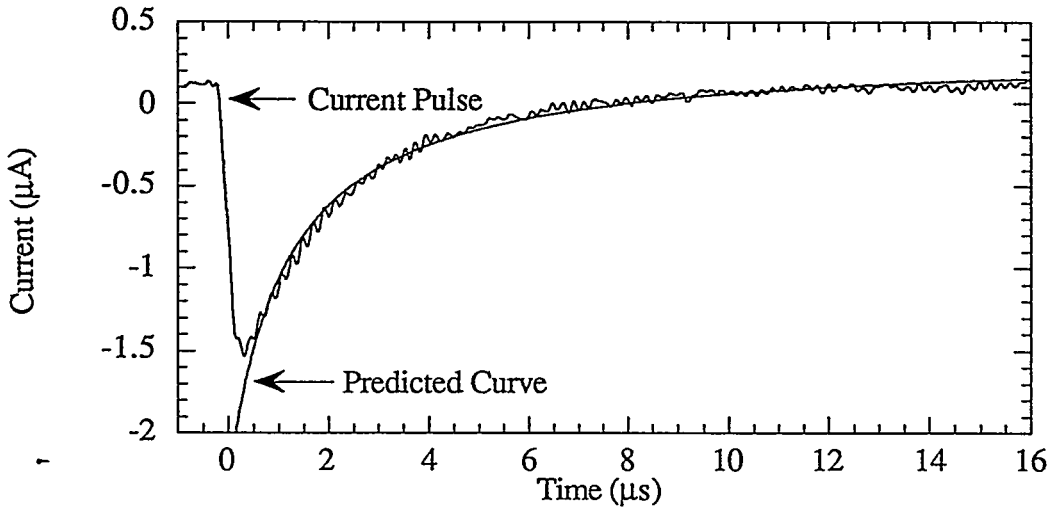

Fig. 2: A typical current pulse has been fit by the self-recombination only model. The figure shows the best fit decay curve and the current pulse for comparison. The pulse has been smoothed to better reveal its shape. The predicted curve deviates from the actual curve in a number of places. Our electronics have inverted the current pulse.

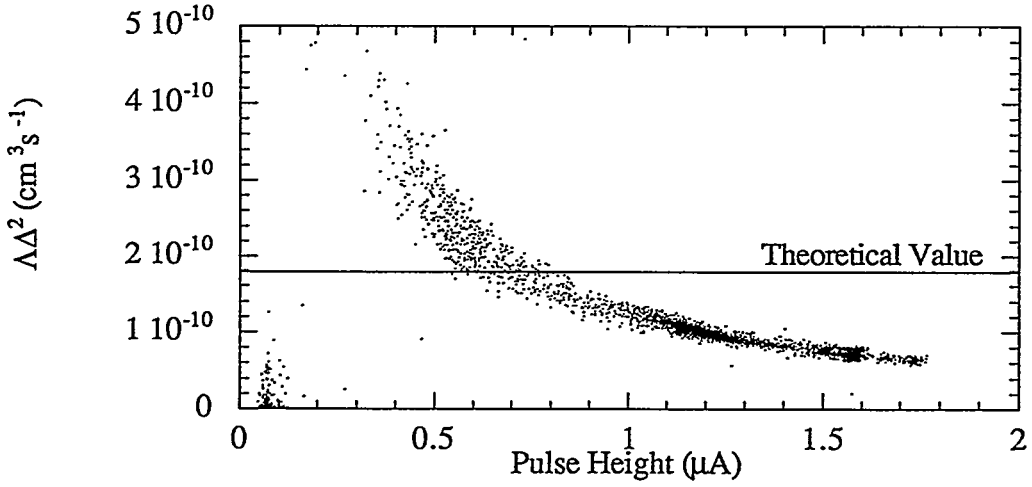

Fig 3: The self-recombination coefficient computed from a fit of the self-recombination only model to a collection of pulses is plotted against the pulse height. According to the model, $\Lambda\Delta^2$ should depend only on the operating conditions and detector geometry. This shows that self-recombination is not sufficient to model the decay of the current pulse. The points near the origin are triggers on electronic noise. The theoretical value calculated from material constants is also shown.

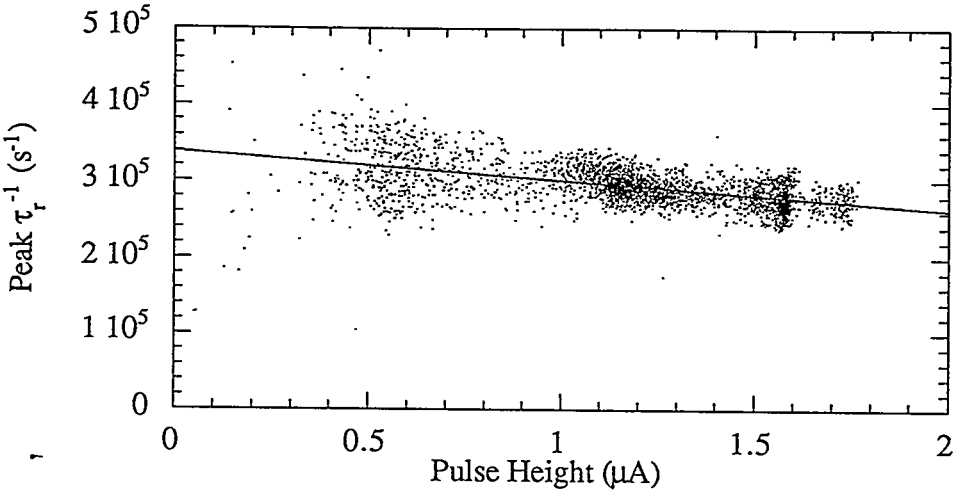

Fig. 4: The self-recombination coefficient obtained from the self-recombination only model has been multiplied by the quasiparticle density and plotted against the peak pulse height. A linear dependence of this quantity on pulse height is apparent. A horizontal line would correspond to a pure exponential decay, while a sloped line with intercept at zero would correspond to a 1/t decay. This plot indicates the actual decay is a combination of the two. The line shown is a linear fit to the data, which can be related to an average pulse decay shape.

the peak quasiparticle density n computed from the current. This quantity is the inverse recombination time τ_r^{-1} previously mentioned, measured at the peak of the pulse. Figure 4 shows τ_r^{-1} plotted against the pulse height. Since the pulse height is proportional to peak quasiparticle density, τ_r^{-1} is a linear function of n. With this dependence, equation (1) becomes:

$$\frac{dn}{dt} = -2\left(c_1 + \frac{c_2}{2eN(0)R_N}n\right)n \ , \qquad (9)$$

where c_1 and c_2 are the respective y-intercept and slope of the line shown in Fig. 4. Comparing with the complete model of equation (5) shows that this dependence is equivalent to having both self-recombination and unwanted trapping mechanisms. A linear fit through these data provides an estimate of τ^{-1}_{loss} and $\Lambda\Delta^2$. If the slope, c_2, was zero (a horizontal line) then the pulse decay would be exponential, indicating only unwanted trapping losses. On the other hand, if the intercept, c_1, is zero, then the decay is due to self-recombination. The plot in Fig. 4 indicates that neither model alone is consistent with the data. The negative slope in Fig. 4 indicates that the larger pulses tend to decay more slowly, contrary to the predictions of our simple model. One should note that this estimate does not correspond to a fit of an actual pulse with two parameters, but is inferred from the behavior of a large number of pulses. It is necessary to use a more complete model to fit the pulse shape more accurately and separate these two mechanisms.

4.2. Self-recombination and unwanted trapping model

Since the current pulse shape could not be modeled by self-recombination alone, we repeated the fits using the more complicated model in equations (5) and (6). Estimates of τ^{-1}_{loss} and $\Lambda\Delta^2$ were calculated from the fits. These quantities were plotted against the peak pulse height in Fig. 6a and 6b.

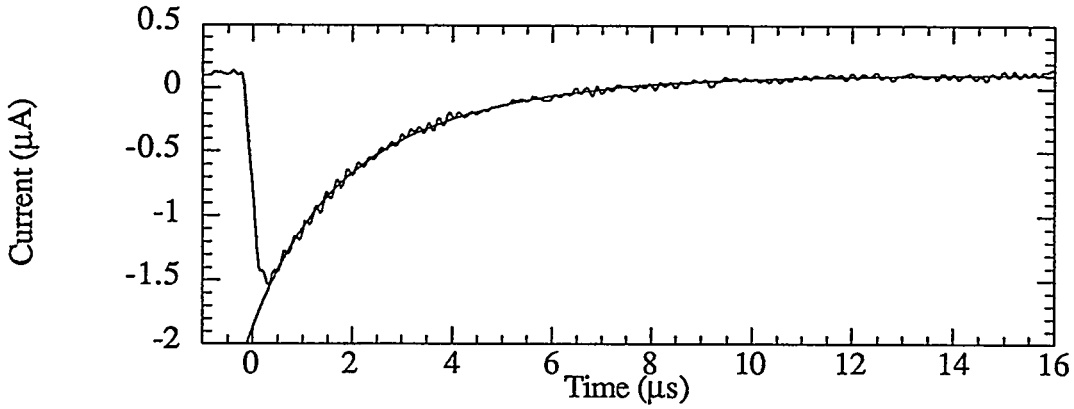

Fig. 5: The current pulse from Fig. 2 now fit to the model that includes both self-recombination and unwanted trapping losses. The model fits the decay excellently.

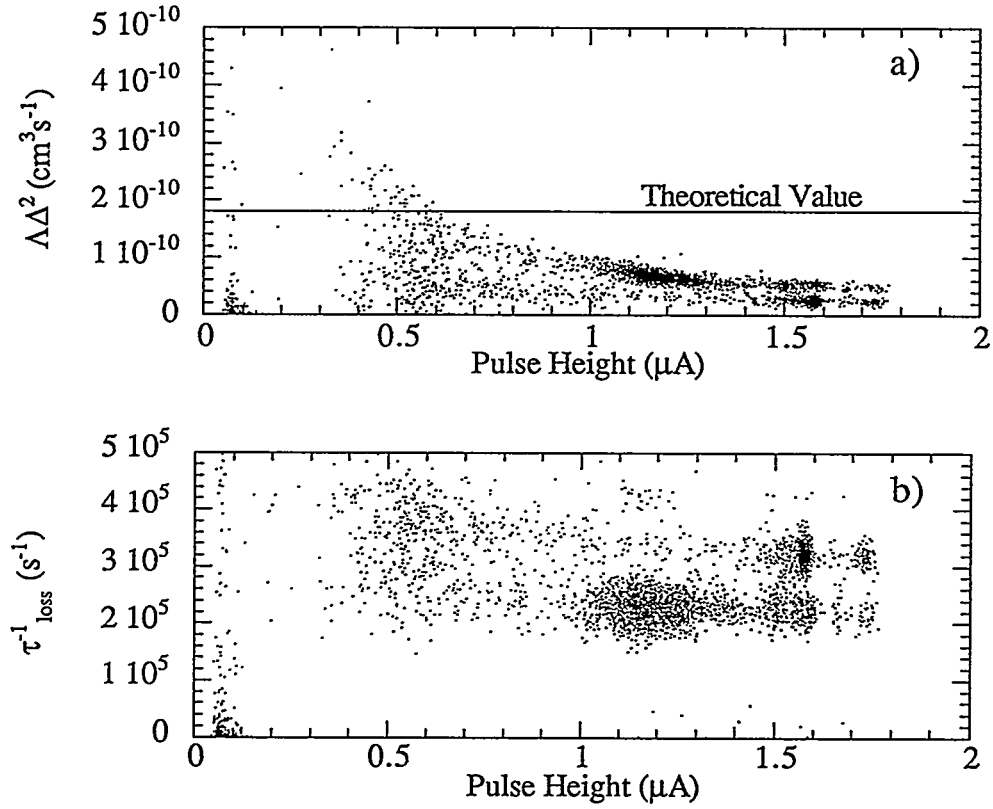

Fig 6: a) The self-recombination coefficient calculated from the complete model is shown plotted against the peak pulse height. As with the model shown in Fig. 3, there is also some amplitude dependence. However, not all the points are constrained to a single band as before. Also, there appears to be two distinct sets of data with different values of $\Lambda\Delta^2$. Again, the low amplitude pulses are noise triggers. The theoretical value calculated from material constants is also shown. b) The trapping loss rate is shown plotted against the peak pulse height. The value of τ^{-1}_{loss} is nearly constant as expected. It also shows a dramatic separation between the two sets of pulses. Note that the set with the larger $\Lambda\Delta^2$ value has the smaller τ^{-1}_{loss} value, and vice versa.

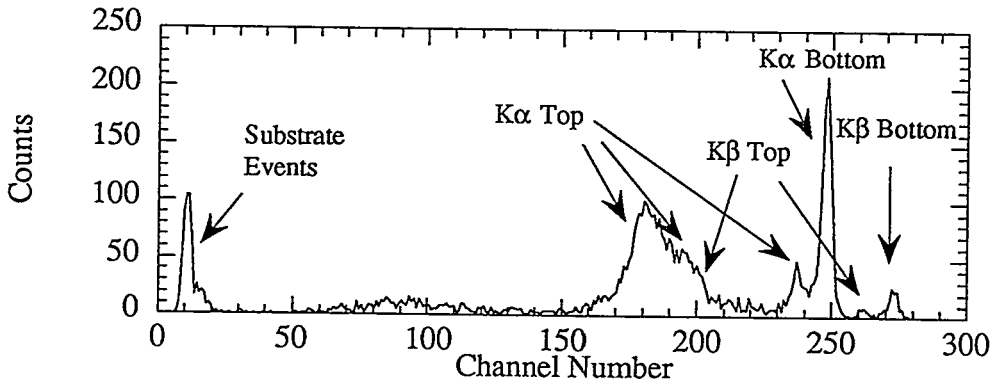

Fig 7: This is a spectrum generated from the data analyzed in this paper. The origin of each feature is explained in the text.

As in the fit using the previous model, the estimated value for $\Lambda\Delta^2$ is not constant. However, its deviation from a constant is not as pronounced as it was in the previous calculation. Also, points are scattered between a 1/n curve as an upper bound and a constant as a lower bound. We believe that the minimum in χ^2 space for these two parameters is very shallow and the fitting algorithm is selecting between sets of decay parameters with nearly the same χ^2. A detailed calculation of the χ^2 space has not been done at this time.

The value for the self-recombination coefficient for most of the pulses falls between 2×10^{-11} cm^3s^{-1} and 1×10^{-10} cm^3s^1. This is a factor of 2 to 8 slower than the theoretical value. Given the many approximations used in the theoretical calculations, and the many parameters used in the fit, we consider this to be an encouraging result. This value is positive, as expected by our model, so the the variation of the overall decay rate with pulse height shown in Fig. 4 is due to another unknown factor. Also, the calculated value of τ^{-1}_{loss} is nearly constant, as expected by our model. One should note that the phonon produced during recombination can break a Cooper pair before leaving the aluminum. This has the effect of extending the observed lifetime or reducing the effective recombination rate of the quasiparticle distribution. If this is the case, these measurements suggest only 1 in 8 such phonons actually escape from the aluminum.

Both parameters exhibit a splitting of the data points. One set has a larger self-recombination rate and smaller trapping loss rate, while the other is the opposite. The distribution of pulse heights, τ^{-1}_{loss}, and $\Lambda\Delta^2$ remained constant over the time the data were taken, indicating that the variations in the values of τ^{-1}_{loss} and $\Lambda\Delta^2$ are not due to a change in the operating conditions.

The origin of the pulses can be determined by comparing Fig. 6 to a spectrum generated from the pulse height data. This spectrum is shown in Fig. 7, along with the type and location each feature is believed to have originated from. The two peaks at channels 248 and 274 correspond to the manganese Kα and Kβ lines and originated in the bottom niobium layer. The irregular structure between channels 165 and 240 and the peaks at channels 247 and 261 originate in the upper niobium layers. This assignment was made on the basis that the largest number of counts, which are found in the unresolved peaks in the middle of the graph should originate in the largest absorber. The lack of any resolved peaks in from these counts may be due to granularity in the thick niobium absorber or to a poor interface between the two top layers of niobium.

We used the splitting shown in Fig. 6b to generate two separate spectra, one believed to originate in the top niobium layers, the other in the bottom niobium layer. The first set, shown in Fig. 8a, had values of τ^{-1}_{loss} between 2.75×10^5 cm^3s^{-1} and 3.75×10^5 cm^3s^{-1}, and is believed to have originated in the bottom

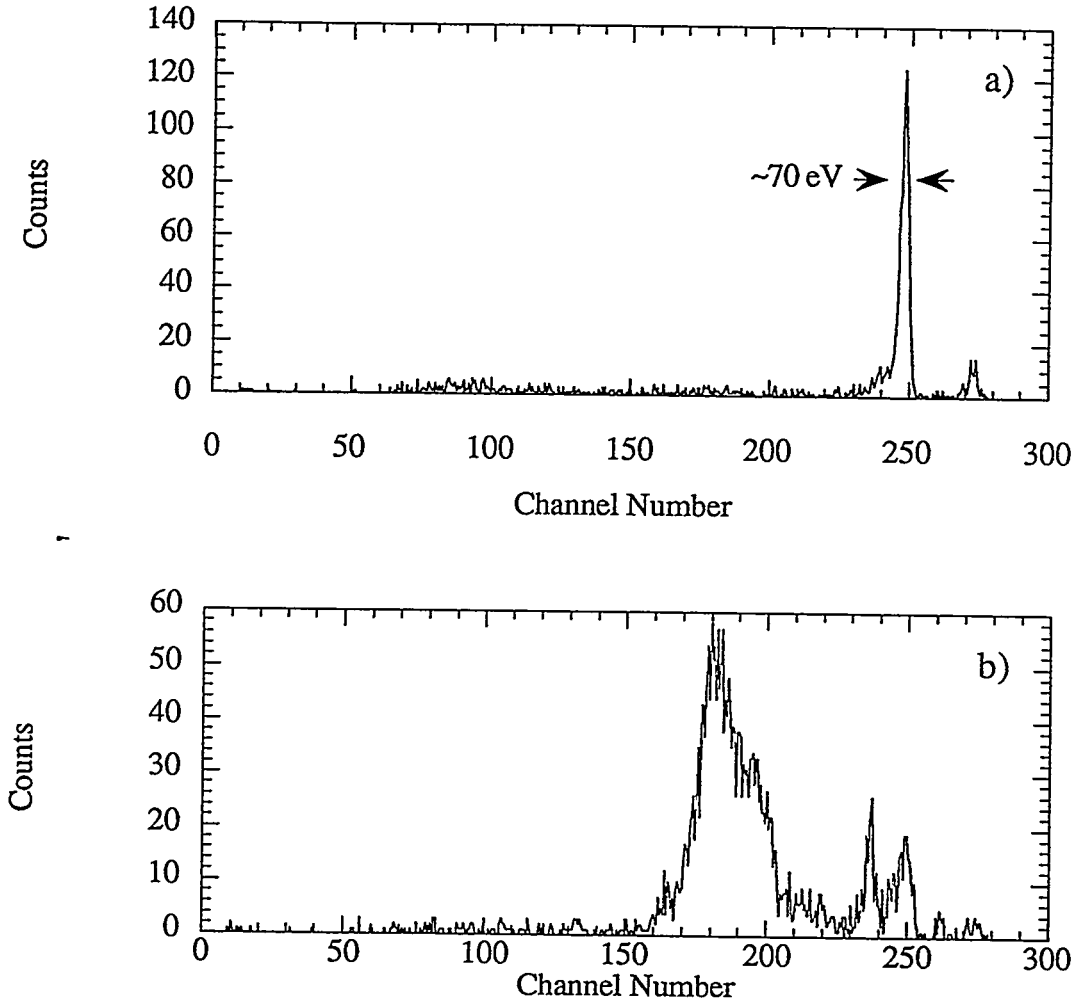

Fig 8: a) Spectrum generated from pulses with a τ^{-1}_{loss} between 2.75×10^5 cm^3s^{-1} and 3.75×10^5 cm^3s^{-1}. These pulses are believed to originate in the bottom niobium layer. b) Spectrum generated from pulses with a τ^{-1}_{loss} between 1.75×10^5 $cm^3s^{-1}$and 2.75×10^5 cm^3s^{-1}. These pulses are believed to originate in the top niobium films.

niobium layer. The second, shown in Fig. 8b, had values of τ^{-1}_{loss} between 1.75×10^5 cm^3s^{-1} and 2.75×10^5 cm^3s^{-1} and is believed to have originated in the top niobium layers. By separating the data in this manner, we have completely eliminated the overlap from the top niobium layers in Fig 8a. The asymmetric shape of the Kα peak is the same as those from other detectors that do not suffer from overlapping spectra. The spectral resolution shown in Fig. 8a is about two times broader than what we have achieved with similar devices.[3] The extra width in this measurement is due to our use of a non-optimal shape-preserving filter.

We also fit these data with a single exponential decay model, and a splitting similar to that shown in Fig. 6 was observed. This revealed that the pulses associated with the bottom layer had a slightly faster decay than those associated with the top layers. These are measurements of the quasiparticle lifetime in the aluminum, and should not be sensitive to which niobium layer the X ray is absorbed. We have considered a few possible explanations for this. 1) Temporary trapping or long distance diffusion in the topmost niobium layer cause it to act as a long-lasting source. 2) Multiple tunneling does not occur. The quasiparticles tunnel only from the aluminum layer adjacent to the layer in which they were absorbed, and each aluminum layer is slightly different. 3) A difference between the aluminum-niobium interface on the

two sides that affects the trapping of the quasiparticles. In the first case, we cannot eliminate the possibility of trapping in the niobium films. However, we have estimated the mean free path in the niobium to be about 30 nm, so quasiparticles should diffuse the maximum thickness of the niobium in 160 ps. Therefore, the niobium should not act as a source on the time scale of our measurements. In the second case, we have calculated the everage time for a quasiparticle to tunnel for our 200 nm aluminum traps to be 1.2 μs.[6,10] Since the apparent lifetime is roughly 2 μs, it is likely that the quasiparticles are not evenly distributed between the two aluminum layers during the current pulse. The third case also remains a likely possibility.

It should be noted that devices without the additional absorbing layer generate only two pairs of peaks; one originating in the top and one in the bottom niobium layer. Peaks associated with the lower layer are shifted downwards in energy due to phonons escaping into the substrate. These peaks are individually well resolved, but often are overlapping. This pulse fitting technique will permit us to separate poorer resolution peaks originating in one layer from the desired peaks in another.

5. CONCLUSIONS

We have shown that the decay of the current pulse output by an STJ detector when it absorbs an X ray is best modeled when both a loss proportional to the quasiparticle density and a lost proportional to the square of the density are considered. The loss proportional to the density corresponds to a number of geometric effects, such as trapping in depressed gaps and normal regions. The loss proportional to the square of the density corresponds to the self-recombination of the excited quasiparticles.

We developed an approximate expression for the proportionality constant for self-recombination which we termed the self-recombination coefficient. The value calculated from this expression is 2 times larger than the value computed from our decay model. This factor suggest that in our devices, when two quasiparticles recombine the phonon released usually breaks Cooper pairs, and is only truly lost about 12% of the time. Our model should be reformulated to include the branch mixing between phonons and quasiparticles, and to include geometrical effects such as phonon escape.

The fitting revealed a small, but well-defined difference in the shape of pulses originating on different sides of the tunnel barrier. By selecting pulses with decay parameters in a certain range, a spectrum could be generated from absorption events originating in a single layer. The result was a clean spectrum that resembled spectra from other devices that did not have overlapping peaks.

6. ACKNOWLEDGMENTS

We would like to thank R. C. Dynes and John Clarke for useful discussions. This work was performed under the auspices of the U. S. Department of Energy by Lawrence Livermore National Laboratory under contract No. W-7405-ENG-48 with additional support from NASA contract NAS5-38013 and NASA grant number NAGW-3907.

7. REFERENCES

1. M. Kurakado, "Possibility of high resolution detectors using superconducting tunnel junctions," *Nucl. Inst. and Meth.*, Vol. 196, pp. 275-277, 1982.

2. N. Rando, *et al.*, "The properties of niobium superconducting tunneling junctions as X-ray detectors," *Nucl. Inst. and Meth.*, Vol. 313, pp. 173-195, 1992.

3. C. A. Mears, Simon E. Labov, and A. T. Barfknecht, "High-resolution superconducting X-ray detectors with two aluminum traps," *Journal of Low Temperature Physics*, Vol. 93, (3/4), pp. 561-566, 1993.

4. Booth, "Quasiparticle trapping and the quasiparticle multiplier," *Appl. Phys. Lett.*, Vol. 50 (5) pp. 293-295, 1987.

5. Kenneth E. Gray, *Applied Physics Letters*, Vol. 32, pp. 392, 1978.

6. C. A. Mears, Simon E. Labov, and A. T. Barfknecht, "Energy-resolving superconducting x-ray detectors with charge amplification due to multiple quasiparticle tunneling," *Appl. Phys. Lett.*, Vol. 61 (21), pp. 2961-2963, 22 November 1993.

7. A. T. Barfknecht, R. C. Ruby, and H. Ko, "A simple and robust niobium josephson junction integrated circuit process," *IEEE Trans. Magn.*, Vol. MAG-27, pp. 970-973, 1991.

8. Kaplan, *et al.*, "Quasiparticle and phonon lifetimes in superconductors," *Phys. Rev. B*, Vol. 14, pp. 4854-4893, 1 Dec. 1976.

9. C. C. Chi and John Clarke, "Quasiparticle branch mixing rates in superconducting aluminum," *Phys. Rev. B*, Vol. 19 (9), 1 May 1979.

10. P. A. J. de Korte, et al., "Superconductive tunnel junctions for x-ray spectroscopy," *Proceedings of the SPIE*, Vol. 1743, July, 1992.